Luminescent Hosts

International Edition: DOI: 10.1002/anie.201501670
German Edition: DOI: 10.1002/ange.201501670

# Bright Fluorescence and Host–Guest Sensing with a Nanoscale $M_4L_6$ Tetrahedron Accessed by Self-Assembly of Zinc–Imine Chelate Vertices and Perylene Bisimide Edges**

*Peter D. Frischmann, Valentin Kunz, and Frank Würthner**

***Abstract:*** *A highly luminescent $Zn_4L_6$ tetrahedron is reported with 3.8 nm perylene bisimide edges and hexadentate $Zn^{II}$–imine chelate vertices. Replacing $Fe^{II}$ and monoamines commonly utilized in subcomponent self-assembly with $Zn^{II}$ and tris(2-aminoethyl)amine provides access to a metallosupramolecular host with the rare combination of structural integrity at concentrations $<10^{-7}$ mol $L^{-1}$ and an exceptionally high fluorescence quantum yield of $\Phi_{em}=0.67$. Encapsulation of multiple perylene or coronene guest molecules is accompanied by strong luminescence quenching. We anticipate this self-assembly strategy may be generalized to improve access to brightly fluorescent coordination cages tailored for host–guest light-harvesting, photocatalysis, and sensing.*

Development of predictable directional bonding interactions for multi-component self-assembly has dramatically simplified access to highly ordered, functional architectures.[1] Supramolecular coordination complexes (SCCs) such as two-dimensional macrocycles and three-dimensional cages are of particular interest because they often exhibit emergent host–guest phenomena.[2] Desirable photophysical properties such as light-harvesting,[3] long-lived charge-separated state lifetimes,[4] encapsulation assisted proton-coupled electron transfer,[5] emission tuning,[6] small-molecule sensing,[7] biological imaging,[8] and photoresponsive guest uptake/release[9] have been realized by integrating emissive ligands and/or coordination complexes into metallosupramolecular macrocycles and cages. Despite these impressive accomplishments, a majority of SCCs exhibit weak or completely quenched emission owing to energy or electron transfer between the excited state and the intrinsic metal ions, resulting in non-radiative relaxation.[10] The ligand-field stabilization provided by open d-shell transition metals, often essential to access kinetically inert SCCs, comes at the price of emission efficiency. A few exceptional cases of highly luminescent metallosupramolecular macrocycles and cages have been documented such as BODIPY-Pt metallomacrocycles,[11] $Pd_2L_4$ cages,[12] and $Zn_2L_4$ cages.[13] Improved access to robust SCCs with enhanced quantum yields will correlate directly with increased utility of these fascinating materials.

Herein we describe our discovery of a PBI-based tetrahedron with zinc–imine chelate vertices, **T** (Scheme 1), that exhibits strong luminescence and host–guest interactions with polycyclic aromatic guests, resulting in excited-state emission quenching. Importantly, the metallosupramolecule is structurally robust even at concentrations below $10^{-7}$ mol $L^{-1}$ as required for the majority of fluorescence-based applications. We envision that the chelate strategy presented here to replace emission quenching $d^6$ $Fe^{II}$ with photophysically benign $d^{10}$ $Zn^{II}$ in subcomponent self-assembly may be generalized to access a variety of often elusive kinetically stable and highly emissive SCCs.

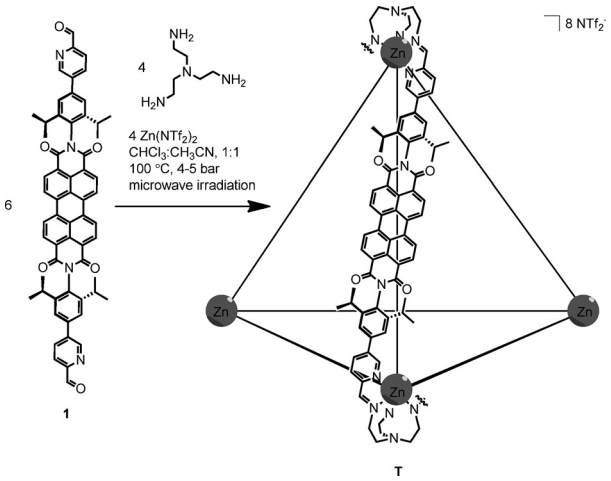


***Scheme 1.*** Self-assembly of tetrahedron **T** from PBI **1**, tris(2-aminoethyl)amine (TREN), and $Zn(NTf_2)_2$.

In a previous effort to wed the electro- and photo-active properties of perylene bisimide (PBI) dyes[14] with metallosupramolecular host–guest chemistry, we reported a giant $Fe_4L_6$ tetrahedron based on PBI ligands that exhibits impressive stability, redox chemistry (reversible cycling of 34 electrons), and is capable of encapsulating up to two $C_{60}$ guests.[15] Although the host absorbs strongly in the visible region, the strong fluorescence that is characteristic of PBI dyes was completely quenched owing to the incorporation of $Fe^{II}$ vertices that are known to promote intersystem crossing and non-radiative relaxation. On the other hand, subcomponent self-assembly of similar PBI-based ligands with *p*-anisidine and $Zn^{II}$ instead of $Fe^{II}$ was hampered by the low thermody-

[*] Dr. P. D. Frischmann, V. Kunz, Prof. Dr. F. Würthner
Institut für Organische Chemie and Center for Nanosystems Chemistry, Universität Würzburg
Am Hubland, 97074 Würzburg (Germany)
E-mail: wuerthner@chemie.uni-wuerzburg.de

[**] P.D.F. thanks the Alexander von Humboldt Foundation for a postdoctoral fellowship. Generous financial support by the DFG (FOR 1806 "Light-induced Dynamics in Molecular Aggregates") is gratefully acknowledged.

Supporting information for this article is available on the WWW under http://dx.doi.org/10.1002/anie.201501670.

  

namic and kinetic stability of the metallosupramolecular tetrahedron that disassembled at low concentrations preventing detailed photophysical study.[16]

To overcome the lability of Zn–N coordination chemistry and construct a brightly fluorescent and robust SCC, we introduced tris(2-aminoethyl)amine (TREN) as the amine source in subcomponent self-assembly with $Zn(NTf_2)_2$ and **1** to yield hexadentate zinc–imine chelate complexes as vertices in the final tetrahedral assembly. Microwave heating of all three components in $CH_3CN$:$CHCl_3$ (1:1) at 100 °C and 4–5 bar for 2 h followed by size-exclusion chromatography afforded the self-assembled tetrahedron **T** from 14 components in one pot and 92 % yield (Scheme 1). The tris-amine TREN is essential to isolate a robust product as similar reactions with *p*-anisidine yielded a tetrahedron that disassembles at low concentration.[16] Although **T** could be isolated using conventional conductive heating, the reaction times were significantly longer (24–72 h).[17]

ESI-MS analysis of the tetrahedron in $CH_3CN$ revealed very sharp signals found at $m/z = 769.54$, 919.47, 1119.37, 1399.22, 1819.26 and assigned to $\mathbf{T}^{8+}$, $\mathbf{T}(NTf_2)^{7+}$, $\mathbf{T}(NTf_2)_2^{6+}$, $\mathbf{T}(NTf_2)_3^{5+}$, and $\mathbf{T}(NTf_2)_4^{4+}$, respectively (Figure 1). Each peak exhibits a perfect isotopic distribution fingerprint, and the $\mathbf{T}^{8+}$ peak with signature 0.125 $m/z$ spacing is depicted in Figure 1 b as a representative spectrum.

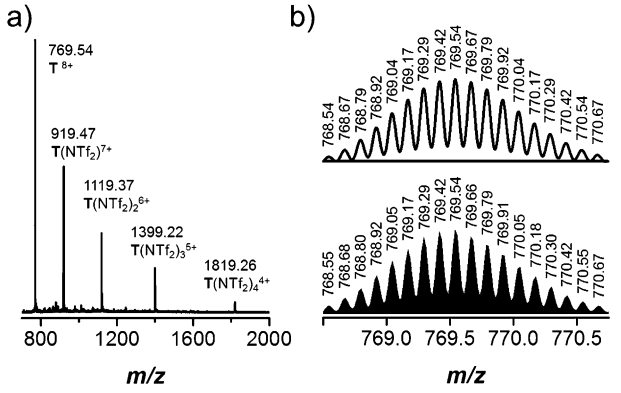


***Figure 1.*** a) ESI-MS of **T**. b) Simulated (top) and experimental (bottom) isotopic distributions of $\mathbf{T}^{8+}$.

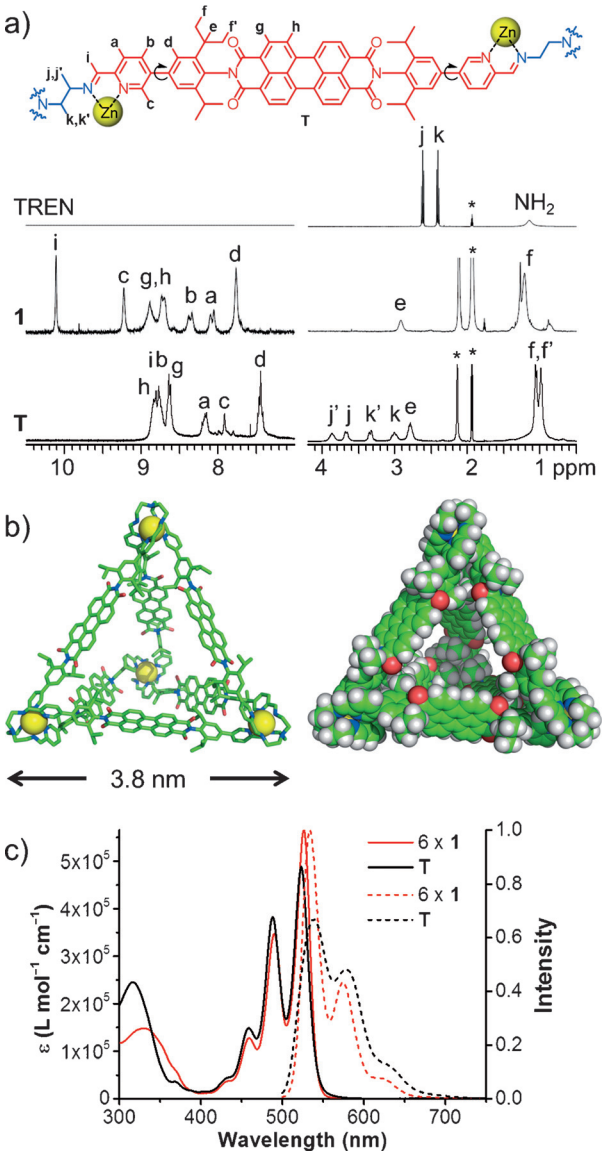


***Figure 2.*** a) $^1$H NMR spectra in $CD_3CN$ of TREN, **1**, and **T**; above is the structure of the PBI tetrahedron edge with proton labels and bonds that rotate freely at elevated temperature indicated. b) Stick and space-filling MMFF geometry optimized structures of **T** as the ΔΔΔΔ diastereomer (C green, N blue, O red, H white, Zn yellow). c) Absorption (——) and emission (-----) spectra of **1** and **T** in $CH_3CN$ ($\lambda_{exc} = 490$ nm). The spectra of **1** are multiplied by six for comparison.

Self-assembly of **T** gives rise to changes in the chemical shifts in the $^1$H NMR spectrum for all proton resonances, as shown in Figure 2 a. The absence of downfield aldehyde and free $NH_2$ resonances supports in situ imine condensation. Protons c and d exhibit significant upfield shifts up to 1.3 ppm for c while less dramatic but noticeable shifts are also observed for a, b, and PBI core protons g and h. The two methylene proton environments of TREN, j and k, shift downfield and split into four diastereotopic resonances, j/j′ and k/k′, upon self-assembly, confirming the chiral nature of the zinc–imine chelate vertices. Additionally, the single resonance of the *i*Pr methyl group, f, of PBI **1** shifts upfield and splits into two diastereotopic resonances, f and f′. All protons were identified through a combination of 2D $^1$H–$^1$H COSY, $^1$H–$^1$H ROESY, and $^1$H–$^{13}$C HSQC (see the Supporting Information). The chemical shifts assigned to the $Zn^{II}$ vertices of **T** are similar to those of a comparable hexadentate zinc–imine chelate complex.[18] A $^1$H DOSY spectrum confirmed that all of the resonances belong to a single species with a diffusion coefficient of $4.0 \times 10^{-10}$ m$^2$ s$^{-1}$, and an experimental hydrodynamic radius of $R_H = 2.2$ nm calculated with the Stokes-Einstein equation for a spherical assembly (Supporting Information, Figure S1).

A molecular force field MMFF geometry optimization of **T** was performed to corroborate the structural details of **T**, and the result is depicted in Figure 2 b.[19] The optimized structure of **T** has 3.8 nm edges, 3.0 nm Zn–Zn distances, 1.5 and 2.0 nm adjacent and opposing PBI–PBI distances, respectively (measured from centroids), and 1.0 nm diameter

apertures. A calculated 1.9 nm radius is in close agreement with the $R_H$ determined by DOSY NMR. The large apertures make the internal volume difficult to define exactly; however, a conservative estimate places the cavity volume around 1300 Å$^3$ with a roughly spherical void space.

Because the PBI tetrahedron edges are exceptionally long and thus more flexible, we anticipated minimal chirality transfer between Δ and Λ octahedral vertices similar to $Fe_4L_6$ tetrahedra reported by Nitschke and co-workers.[20] $Fe_4L_6$ tetrahedra with shorter edges exhibit diastereomerism arising from weak chirality transfer even when enantiopure amines are applied in subcomponent self-assembly.[21] A variable-temperature $^1$H NMR experiment was performed in $CD_3CN$ from 1 to 70 °C to help elucidate the conformational state of the system. Upon heating, all of the resonances sharpen considerably (Supporting Information, Figure S2), and the process is completely reversible upon cooling. No decomposition was observed even after heating the sample at 50 °C for 16 h, emphasizing the integrity of the zinc–imine chelate vertices for constructing future metallosupramolecular architectures. The presence of single resonances for protons e, f, f′, g, and h at elevated temperature confirms that the PBI cores rotate freely about their long axis (see arrows indicating the rotational axis on the structure in Figure 2a). However, some broadening is still observed at high temperature, and multiple resonances assigned to each proton a, b, c, and d are attributed to the ΔΔΔΔ ($T$), ΔΔΔΛ ($C_3$), and ΔΔΛΛ ($S_4$) diastereomers, indicating that a fast-exchange regime could not be reached for diastereomer interconversion. Eight distinct resonances are observed for proton **c**, which is exactly as predicted for the coexistence of $T$, $S_4$, and $C_3$ diastereomers with one, three, and four distinct resonances, respectively (Supporting Information, Figure S3).[20] The diastereomeric resonances of c have been assigned based on the agreement of integrals and the number of distinct resonances yielding an estimated $T$:$S_4$:$C_3$ diastereomeric ratio of 1:0.9:0.7 for **T** in $CD_3CN$ at 50 °C. An imine exchange strategy might be employed in the future to lock in a single tetrahedral diastereomer beginning the assembly with chiral monoamines.[22]

Confirmation that **T** is robust at the low concentrations common for fluorescence spectroscopy came from a variable concentration UV/Vis absorption study where no spectral changes were observed down to $8.3\times10^{-8}$ mol L$^{-1}$ in $CH_3CN$. Absorption and emission spectra of **T** and **1** (×6 for comparison) are depicted in Figure 2c. PBI **1** exhibits characteristic optical properties of a typical bay-unsubstituted PBI dye;[14] however, interesting spectral changes are observed upon tetrahedron formation. Relative to **1** (526 nm, 94300 L mol$^{-1}$ cm$^{-1}$; 490, 57900), self-assembly of **T** (523 nm, 488400 L mol$^{-1}$ cm$^{-1}$; 488, 382300) results in slight blue shifts in the absorption maxima and a 14% decrease of the extinction coefficient for the 0→0 vibronic transition with concurrent 10% and 15% increases for those of the 0→1 and 0→2 vibronic transitions, respectively (compared to 6×**1**). Emission spectra recorded by exciting the 0→1 vibronic transition ($\lambda_{exc}=490$ nm) show larger Stokes shifts and broadened transitions for the tetrahedron ($\lambda_{em}=538$ and 578 nm) compared to **1** ($\lambda_{em}=533$ and 574 nm). Impressively, the fluorescence quantum yield of **T** is $\Phi_{em}=0.67\pm0.02$, making it one of the most emissive metallosupramolecular cages reported. Although free PBI **1** maintains a unity quantum yield, the 33% reduction in emission efficiency is superior to typical quenching observed upon metal-coordination directed self-assembly which is generally in excess of 50% and often approaches 100% quenching.[3e,7b] Both **1** and **T** exhibit $\tau=4.8$ ns excited state lifetimes (Supporting Information, Figures S4, S5). Each PBI dye in **T** is held in close proximity to four other PBI dyes with a 60° angle between the long axes of the dyes where oblique excitonic coupling may be responsible for the observed spectral changes and reduction in emission efficiency.[23]

Polycyclic aromatic hydrocarbons (PAHs) coronene (**C**) and perylene (**P**) were chosen as suitable guest molecules to explore emergent supramolecular host–guest photophysics due to their large π-surfaces that may interact with PBI, complementary absorption spectra (in the case of perylene), and electron rich nature relative to PBI that may enable photoinduced charge transfer. Sonication of **T** with a 20-fold excess of either **C** or **P** in $CD_3CN$ followed by filtration to remove any undissolved PAHs yielded the $^1$H NMR spectra depicted in Figure 3. Distinct upfield shifts are observed for each guest molecule indicative of encapsulation. Concurrently protons g, h, and f of the tetrahedron experience significant upfield chemical shifts, suggesting the guests are located near the *i*Pr groups and PBI cores, thus providing strong evidence for close contact between the π-surfaces of host and guest. Changes upon encapsulation in the chemical shifts of protons assigned to the zinc–imine chelate vertices of

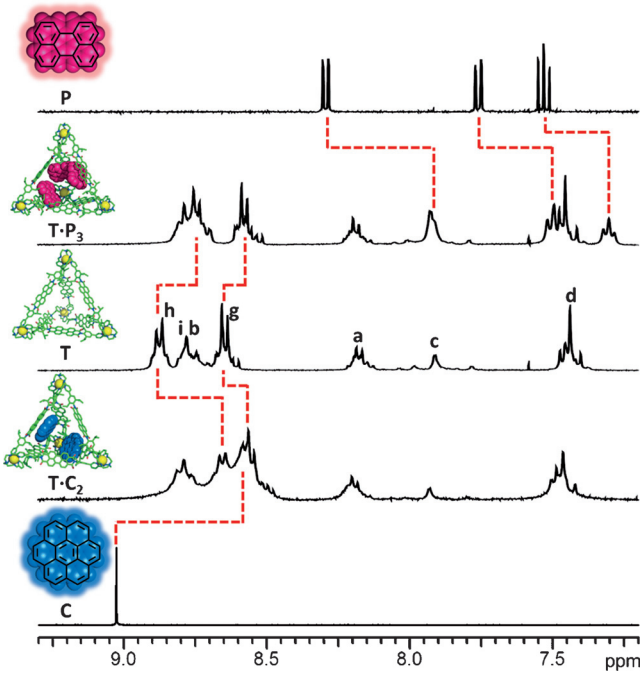


***Figure 3.*** Downfield region of $^1$H NMR spectra with changes due to host–guest encapsulation marked in red for **P**, **T**·**P**$_3$, **T**, **T**·**C**$_2$, and **C** ($CD_3CN$). Resonances of **T** are assigned according to Figure 2a.

  

**T** are minimal. Monitoring changes in the $^1$H NMR titrations established a 1:3 host–guest ratio for **T**:**P** and a 1:2 ratio for **T**:**C** (Supporting Information, Figures S6, S7). Comparing integrals of the isolated perylene resonance at 7.3 ppm and resonance a of the tetrahedron confirms the 1:3 **T**:**P** host–guest ratio. The resonance of encapsulated coronene is convoluted with resonances of **T**; however, the increase in the integral of the downfield region (9.0 to 8.4 ppm) relative to integrals of resonances a, c, and d is commensurate with a 1:2 **T**:**C** ratio.

A single experimental hydrodynamic radius ($R_H = 2.2$ nm) was measured for a solution of $\mathbf{T}\cdot\mathbf{C}_2$ by $^1$H DOSY NMR spectroscopy, indicating the host–guest complex is tightly bound on the NMR timescale (Supporting Information, Figure S8; $R_H$ of **C** = 0.3 nm, Figure S9). In contrast to $\mathbf{T}\cdot\mathbf{C}_2$, the host–guest complex $\mathbf{T}\cdot\mathbf{P}_3$ exhibits separate diffusion coefficients for **T** and **P** corresponding to $R_H = 2.0$ and 1.0 nm, respectively (Supporting Information, Figure S10). A much lower $R_H = 0.3$ nm was measured for free **P** (Supporting Information, Figure S11). Signal averaging of a molecule in equilibrium between two states with different diffusion coefficients is a common phenomenon observed by DOSY NMR spectroscopy.[24] The observed signal averaging of bound and unbound **P** may be rationalized by rapid guest exchange in and out of **T**. Host–guest complexation was further confirmed by ESI-MS where perfect isotopic distributions are observed at $m/z =$ 844.57 for $\mathbf{T}\cdot\mathbf{C}_2^{8+}$ and $m/z = 1027.66$ for $\mathbf{T}\cdot\mathbf{P}_3\cdot(NTf_2)^{7+}$ (Supporting Information, Figures S12, 13).

Host–guest complexation was further established by UV/Vis spectroscopy where bathochromic shifts and decreases in optical density of PBI-derived absorptions are observed for both $\mathbf{T}\cdot\mathbf{C}_2$ and $\mathbf{T}\cdot\mathbf{P}_3$ compared to free **T** as depicted in Figure 4a,b ($6.0\times10^{-4}$ mol L$^{-1}$ **T**). Changes in the PBI absorption upon guest encapsulation suggest that electron-rich **C** and **P** guests favor interacting with the electron poor PBI walls of the cage over homo-aggregation. Molecular force field geometry optimization of $\mathbf{T}\cdot\mathbf{C}_2$ and $\mathbf{T}\cdot\mathbf{P}_3$ show host–guest π-stacking between PBI and coronene or perylene are geometrically reasonable (Supporting Information, Figures S14, S15). UV/Vis spectra of the same $\mathbf{T}\cdot\mathbf{C}_2$ and $\mathbf{T}\cdot\mathbf{P}_3$ solutions diluted to $1\times10^{-6}$ mol L$^{-1}$ exhibit complete recovery of the initial **T** absorption intensity indicating dissociation of the host–guest complex. Low-concentration absorption spectra of dissociated host–guest complexes also enabled further quantification of 1:2 and 1:3 host–guest ratios of $\mathbf{T}\cdot\mathbf{C}_2$ and $\mathbf{T}\cdot\mathbf{P}_3$, respectively (Supporting Information, Figures S16, S17).

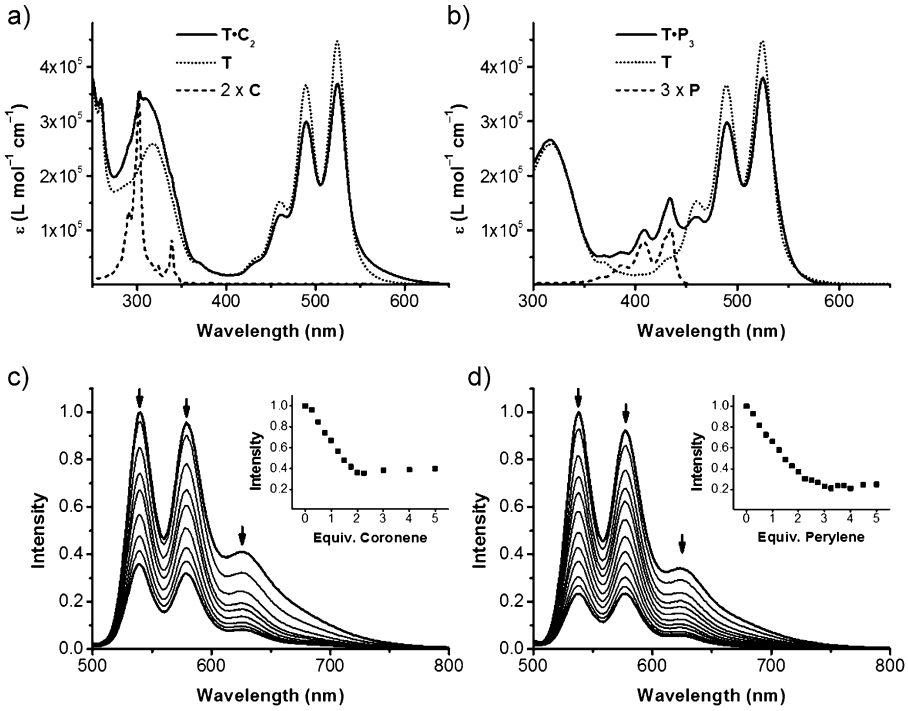


***Figure 4.*** a) Absorption spectra of $\mathbf{T}\cdot\mathbf{C}_2$, **T**, and 2×**C**. b) Absorption spectra of $\mathbf{T}\cdot\mathbf{P}_3$, **T**, and 3×**P**. c) Emission spectra following the titration of **C** into **T**. d) Emission spectra following the titration of **P** into **T**. Insets in (c) and (d) show fluorescence intensity versus equivalents of guest, and arrows indicate changes with increasing concentration of guest. All spectra were measured with **T** at $6.0\times10^{-4}$ mol L$^{-1}$.

Emission quenching of **T** by **C** and **P** is observed upon encapsulation, thus laying the foundation for developing host–guest fluorescence sensors[7] and supramolecular photosystems.[3e–f,4,25] Fluorometric titrations depicted in Figure 4c and d show a steady decrease in fluorescence intensity down to a minimum of 35 and 20% of **T** with the addition of two equivalents of **C** and three equivalents of **P**, respectively. The importance of encapsulation for detection is emphasized by the fact that additional equivalents of guest beyond $\mathbf{T}\cdot\mathbf{C}_2$ or $\mathbf{T}\cdot\mathbf{P}_3$ do not affect the fluorescence intensity. Stern–Volmer plots of the titration data exhibit positive non-linear slopes attributed to a mix of static and dynamic quenching mechanisms (Supporting Information, Figures S18, S19). Addition of one equivalent of guest molecule (**C** or **P**) results in an approximate 35% decrease in emission, which is equivalent to one guest quenching 2.1 PBI chromophores. This mild amplified quenching response[26] might be attributed to a situation where the embedded guest only quenches those PBI emitters which are in close spatial proximity in the host–guest complex.

In summary, a giant and highly fluorescent $Zn_4L_6$ tetrahedron has been synthesized in excellent yield using a combination of dynamic imine condensation and metal–ligand-directed self-assembly. Access to the brightly fluorescent and exceptionally stable tetrahedron was enabled by replacing monoamines and $Fe^{II}$, which are typically used in subcomponent self-assembly of $M_xL_y$ polyhedra, with the tris-amine TREN and $Zn^{II}$, respectively. Encapsulation of perylene or coronene within **T** triggers host–guest responsive

  

amplified emission quenching. We anticipate that the chelate strategy presented here may be generalized to integrate a wide variety of high performance dyes into SCCs accelerating the development of supramolecular host–guest fluorescence sensing, photocatalysis, and light-harvesting applications.

**Keywords:** chromophores · host–guest systems · luminescence · self-assembly · supramolecular chemistry

**How to cite:** *Angew. Chem. Int. Ed.* **2015**, *54*, 7285–7289
*Angew. Chem.* **2015**, *127*, 7393–7397

[1] a) M. D. Ward, P. R. Raithby, *Chem. Soc. Rev.* **2013**, *42*, 1619–1636; b) R. Chakrabarty, P. S. Mukherjee, P. J. Stang, *Chem. Rev.* **2011**, *111*, 6810–6918; c) C. A. Schalley, A. Lützen, M. Albrecht, *Chem. Eur. J.* **2004**, *10*, 1072–1080.

[2] a) M. Han, D. M. Engelhard, G. H. Clever, *Chem. Soc. Rev.* **2014**, *43*, 1848–1860; b) T. K. Ronson, S. Zarra, S. P. Black, J. R. Nitschke, *Chem. Commun.* **2013**, *49*, 2476–2490; c) N. J. Young, B. P. Hay, *Chem. Commun.* **2013**, *49*, 1354–1379; d) S. De, K. Mahata, M. Schmittel, *Chem. Soc. Rev.* **2010**, *39*, 1555–1575; e) M. Yoshizawa, J. K. Klosterman, M. Fujita, *Angew. Chem. Int. Ed.* **2009**, *48*, 3418–3438; *Angew. Chem.* **2009**, *121*, 3470–3490; f) R. W. Saalfrank, H. Maid, A. Scheurer, *Angew. Chem. Int. Ed.* **2008**, *47*, 8794–8824; *Angew. Chem.* **2008**, *120*, 8924–8956; g) B. J. Holliday, C. A. Mirkin, *Angew. Chem. Int. Ed.* **2001**, *40*, 2022–2043; *Angew. Chem.* **2001**, *113*, 2076–2097; h) D. L. Caulder, K. N. Raymond, *Acc. Chem. Res.* **1999**, *32*, 975–982.

[3] a) N. Karakostas, I. M. Mavridis, K. Seintis, M. Fakis, E. N. Koini, I. D. Petsalakis, G. Pistolis, *Chem. Commun.* **2014**, *50*, 1362–1365; b) P. D. Frischmann, K. Mahata, F. Würthner, *Chem. Soc. Rev.* **2013**, *42*, 1847–1870; c) N. Nagata, Y. Kuramochi, Y. Kobuke, *J. Am. Chem. Soc.* **2009**, *131*, 10–11; d) J. K. Klosterman, M. Iwamura, T. Tahara, M. Fujita, *J. Am. Chem. Soc.* **2009**, *131*, 9478–9479; e) M. R. Wasielewski, *Acc. Chem. Res.* **2009**, *42*, 1910–1921; f) R. F. Kelley, S. J. Lee, T. M. Wilson, Y. Nakamura, D. M. Tiede, A. Osuka, J. T. Hupp, M. R. Wasielewski, *J. Am. Chem. Soc.* **2008**, *130*, 4277–4284.

[4] V. L. Gunderson, A. L. Smeigh, C. H. Kim, D. T. Co, M. R. Wasielewski, *J. Am. Chem. Soc.* **2012**, *134*, 4363–4372.

[5] R. Gera, A. Das, A. Jha, J. Dasgupta, *J. Am. Chem. Soc.* **2014**, *136*, 15909–15912.

[6] a) J. B. Pollock, G. L. Schneider, T. R. Cook, A. S. Davies, P. J. Stang, *J. Am. Chem. Soc.* **2013**, *135*, 13676–13679; b) O. Chepelin, J. Ujma, X. Wu, A. M. Z. Slawin, M. B. Pitak, S. J. Coles, J. Michel, A. C. Jones, P. E. Barran, P. J. Lusby, *J. Am. Chem. Soc.* **2012**, *134*, 19334–19337.

[7] a) P. P. Neelakandan, A. Jiménez, J. R. Nitschke, *Chem. Sci.* **2014**, *5*, 908–915; b) T. Nakamura, H. Ube, M. Shionoya, *Angew. Chem. Int. Ed.* **2013**, *52*, 12096–12100; *Angew. Chem.* **2013**, *125*, 12318–12322; c) S. Shanmugaraju, H. Jadhav, Y. P. Patil, P. S. Mukherjee, *Inorg. Chem.* **2012**, *51*, 13072–13074; d) J. Thomas, *Dalton Trans.* **2011**, *40*, 12005–12016; e) M. Wang, V. Vajpayee, S. Shanmugaraju, Y.-R. Zheng, Z. Zhao, H. Kim, P. S. Mukherjee, K.-W. Chi, P. J. Stang, *Inorg. Chem.* **2011**, *50*, 1506–1512; f) K. Ono, J. K. Klosterman, M. Yoshizawa, K. Sekiguchi, T. Tahara, M. Fujita, *J. Am. Chem. Soc.* **2009**, *131*, 12526–12527.

[8] J. Wang, C. He, P. Wu, J. Wang, C. Duan, *J. Am. Chem. Soc.* **2011**, *133*, 12402–12405.

[9] a) M. Han, R. Michel, B. He, Y.-S. Chen, D. Stalke, M. John, G. H. Clever, *Angew. Chem. Int. Ed.* **2013**, *52*, 1319–1323; *Angew. Chem.* **2013**, *125*, 1358–1362; b) N. Kishi, M. Akita, M. Kamiya, S. Hayashi, H.-F. Hsu, M. Yoshizawa, *J. Am. Chem. Soc.* **2013**, *135*, 12976–12979.

[10] a) J.-S. Chen, G.-J. Zhao, T. R. Cook, K.-L. Han, P. J. Stang, *J. Am. Chem. Soc.* **2013**, *135*, 6694–6702; b) J. B. Pollock, T. R. Cook, P. J. Stang, *J. Am. Chem. Soc.* **2012**, *134*, 10607–10620; c) C. M. Drain, J.-M. Lehn, *J. Chem. Soc. Chem. Commun.* **1994**, 2313–2315.

[11] a) A. Kaloudi-Chantzea, N. Karakostas, F. Pitterl, C. P. Raptopoulou, N. Glezos, G. Pistolis, *Chem. Commun.* **2012**, *48*, 12213–12215; b) A. Kaloudi-Chantzea, N. Karakostas, C. P. Raptopoulou, V. Psycharis, E. Saridakis, J. Griebel, R. Hermann, G. Pistolis, *J. Am. Chem. Soc.* **2010**, *132*, 16327–16329.

[12] A. M. Johnson, O. Moshe, A. S. Gamboa, B. W. Langloss, J. F. K. Limtiaco, C. K. Larive, R. J. Hooley, *Inorg. Chem.* **2011**, *50*, 9430–9442.

[13] Z. Li, N. Kishi, K. Yoza, M. Akita, M. Yoshizawa, *Chem. Eur. J.* **2012**, *18*, 8358–8365.

[14] F. Würthner, *Chem. Commun.* **2004**, 1564–1579.

[15] K. Mahata, P. D. Frischmann, F. Würthner, *J. Am. Chem. Soc.* **2013**, *135*, 15656–15661.

[16] P. D. Frischmann, V. Kunz, V. Stepanenko, F. Würthner, *Chem. Eur. J.* **2015**, *21*, 2766–2769.

[17] C. R. K. Glasson, G. V. Meehan, C. A. Motti, J. K. Clegg, P. Turner, P. Jensen, L. F. Lindoy, *Dalton Trans.* **2011**, *40*, 10481–10490.

[18] A. M. McDaniel, A. K. Rappé, M. P. Shores, *Inorg. Chem.* **2012**, *51*, 12493–12502.

[19] ***Spartan'08*** Wavefunction, Inc. Irvine, CA.

[20] W. Meng, J. K. Clegg, J. D. Thoburn, J. R. Nitschke, *J. Am. Chem. Soc.* **2011**, *133*, 13652–13660.

[21] N. Ousaka, S. Grunder, A. M. Castilla, A. C. Whalley, J. F. Stoddart, J. R. Nitschke, *J. Am. Chem. Soc.* **2012**, *134*, 15528–15537.

[22] A. M. Castilla, N. Ousaka, R. A. Bilbeisi, E. Valeri, T. K. Ronson, J. R. Nitschke, *J. Am. Chem. Soc.* **2013**, *135*, 17999–18006.

[23] M. Kasha, H. R. Rawls, M. A. El-Bayoumi, *Pure Appl. Chem.* **1965**, *11*, 371–392.

[24] Y. Cohen, L. Avram, L. Frish, *Angew. Chem. Int. Ed.* **2005**, *44*, 520–554; *Angew. Chem.* **2005**, *117*, 524–560.

[25] R. Bhosale, J. Míšek, N. Sakai, S. Matile, *Chem. Soc. Rev.* **2010**, *39*, 138–149.

[26] S. W. Thomas III, G. D. Joly, T. M. Swager, *Chem. Rev.* **2007**, *107*, 1339–1386.

Received: February 20, 2015
Published online: April 29, 2015

  